A&A 595, A100 (2016)
DOI: 10.1051/0004-6361/201527995

Astronomy & Astrophysics

Discovery of a faint, star-forming, multiply lensed, Lyman-α blob

G. B. Caminha[1], W. Karman[2], P. Rosati[1], K. I. Caputi[2], F. Arrigoni Battaia[3], I. Balestra[4,5], C. Grillo[6], A. Mercurio[7], M. Nonino[5], and E. Vanzella[8]

[1] Dipartimento di Fisica e Scienze della Terra, Università degli Studi di Ferrara, via Saragat 1, 44122 Ferrara, Italy
e-mail: gbcaminha@fe.infn.it
[2] Kapteyn Astronomical Institute, University of Groningen, Postbus 800, 9700 AV Groningen, The Netherlands
e-mail: karman@astro.rug.nl
[3] European Southern Observatory, Karl-Schwarzschild-Str. 2, 85748 Garching b. München, Germany
[4] University Observatory Munich, Scheinerstrasse 1, 81679 Munich, Germany
[5] INAF−Osservatorio Astronomico di Trieste, via G. B. Tiepolo 11, 34143 Trieste, Italy
[6] Dark Cosmology Centre, Niels Bohr Institute, University of Copenhagen, Juliane Maries Vej 30, 2100 Copenhagen, Denmark
[7] INAF−Osservatorio Astronomico di Capodimonte, via Moiariello 16, 80131 Napoli, Italy
[8] INAF−Osservatorio Astronomico di Bologna, via Ranzani 1, 40127 Bologna, Italy

Received 17 December 2015 / Accepted 30 August 2016

ABSTRACT

We report the discovery of a multiply lensed Lyman-α blob (LAB) behind the galaxy cluster AS1063 using the Multi Unit Spectroscopic Explorer (MUSE) on the Very Large Telescope (VLT). The background source is at $z = 3.117$ and is intrinsically faint compared to almost all previously reported LABs. We used our highly precise strong lensing model to reconstruct the source properties, and we find an intrinsic luminosity of $L_{\mathrm{Ly}\alpha} = 1.9 \times 10^{42}$ erg s^{-1}, extending to 33 kpc. We find that the LAB is associated with a group of galaxies, and possibly a protocluster, in agreement with previous studies that find LABs in overdensities. In addition to Lyman-α (Lyα) emission, we find C IV, He II, and O III] ultraviolet (UV) emission lines arising from the centre of the nebula. We used the compactness of these lines in combination with the line ratios to conclude that the Lyα nebula is likely powered by embedded star formation. Resonant scattering of the Lyα photons then produces the extended shape of the emission. Thanks to the combined power of MUSE and strong gravitational lensing, we are now able to probe the circumgalatic medium of sub-L_* galaxies at $z \approx 3$.

Key words. galaxies: high-redshift – galaxies: star formation – intergalactic medium – galaxies: halos – galaxies: evolution – cosmology: observations

1. Introduction

Understanding important processes involved in galaxy evolution, such as accretion and feedback, is crucial to comprehending the medium surrounding galaxies at high redshift In this light, understanding the nature of the so-called Lyman-α blobs (LABs) provides key elements of the conditions of the circumgalactic medium (CGM) at high redshift. These LABs are extended nebulas of tens to hundreds of kpc with high Lyman-α (Lyα) luminosities of 10^{42} to 10^{45} erg s^{-1} cm^{-2} (e.g. Heckman et al. 1991; Steidel et al. 2000; Matsuda et al. 2011; Cantalupo et al. 2014).

While it has become clear that most LABs reside in over dense regions, such as the protocluster SSA22 where a large number of LABs have been found (e.g. Yamada et al. 2012), the mechanism responsible for extended Lyα emission is still a matter of debate. Although active galactic nuclei (AGNe) are often shown at the centres of LABs (e.g. Geach et al. 2009; Overzier et al. 2013) and several quasi stellar objects (QSO) and high-z radio galaxies (HzRG) show extended Lyα emission, other studies find photoionization by star formation (e.g. Bridge et al. 2013; Ao et al. 2015; Patrício et al. 2016) as a cause for the extended emission. Others suggest that the absence of any clear ioniziation source indicates that cold accretion provides the extended Lyα emission (e.g. Nilsson et al. 2006; Saito et al. 2006, 2008; but see Prescott et al. 2015, for the discovery of a hidden AGN in this sample).

Currently, four different scenarios are proposed for ionization of the blobs (see Arrigoni Battaia et al. 2015a, and references therein). First, an AGN could photoionize the medium, and it has been well established that for some LABs this is the dominant factor (e.g. Geach et al. 2009; Overzier et al. 2013). Second, shocks powered by galaxy-scale outflows could interact with the CGM and the intergalactic medium (IGM) producing the large amount of radiation observed (e.g. Mori & Umemura 2006). The third proposed mechanism is cooling radiation through gravitational collapse (e.g. Yang et al. 2006; Dijkstra & Loeb 2009; Faucher-Giguère et al. 2010), which occurs when extended metal-poor collisionally-excited gas cools down by Lyα emission. Last, if a source, such as a star formation (SF) burst or an AGN, is embedded in a large reservoir of neutral gas, resonant scattering of Lyα photons can extend the originally compact Lyα emission (Dijkstra & Loeb 2008; Hayes et al. 2011; Steidel et al. 2011).

It has been shown that a single mechanism cannot explain the origin of the LABs for all sources. It is therefore important for our understanding of galaxy formation to determine which mechanism is responsible in the different classes of objects. One method to distinguish between the mechanisms is to look at the extent of the C IV and He II emission. Extended C IV and He II emission is expected when photoionization or shocks power the Lyα nebula, while only extended He II emission is expected in case of gravitational cooling. Because He II is not a

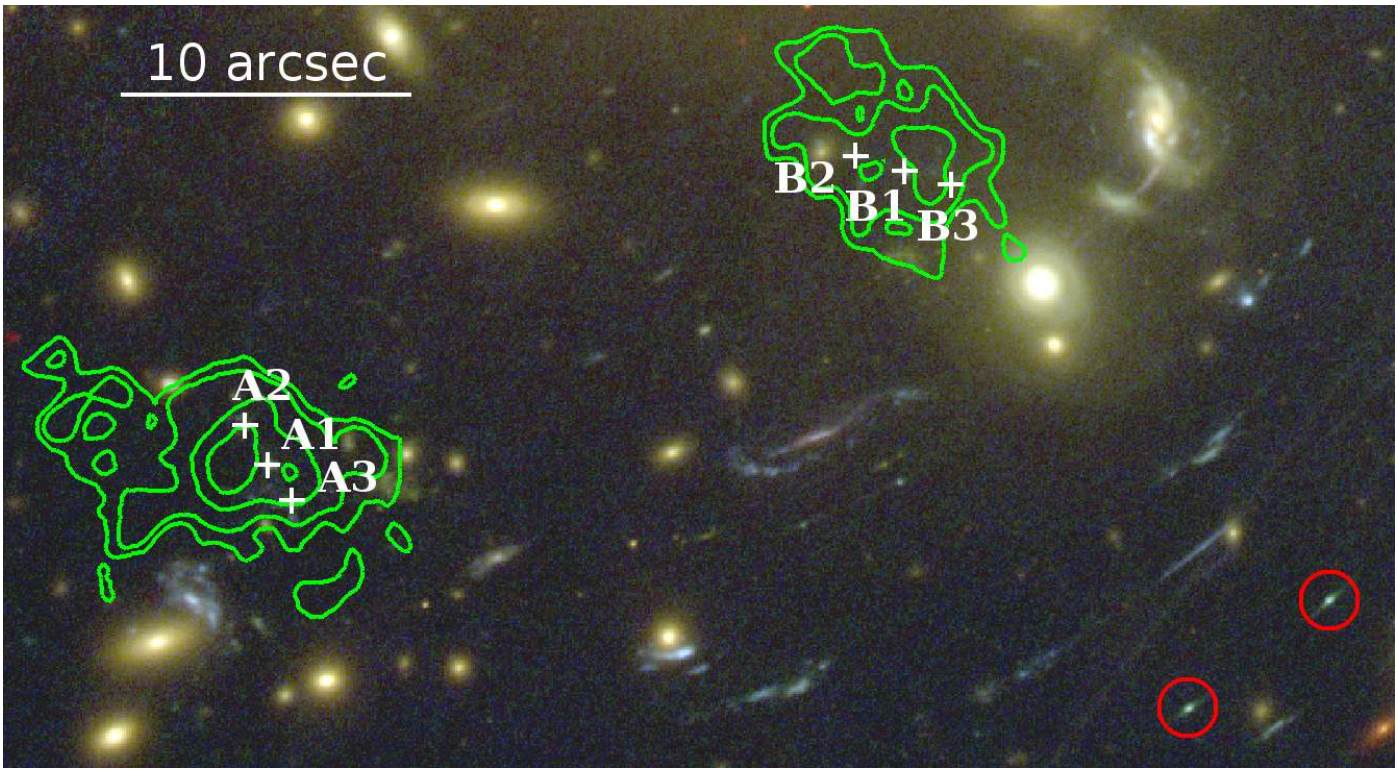

Fig. 1. HFF colour composite image of the south-west region of AS1063 overlaid with Lyα emission isocontours. The white crosses indicate the positions of the three compact sources related to the LAB (as in Fig. 2) and the red circles the multiple images of another galaxy located at the same redshift, studied in detail in Vanzella et al. (2016).

resonant line, no extended He II emission is expected in case of a resonant scattering. Although C IV is resonant, it will only be extended for resonant scattering if the surrounding medium is optically thick to C IV (see Prochaska et al. 2014).

Although extended C IV and He II emission are detected around HzRGs (Villar-Martín et al. 2003, 2007; Humphrey et al. 2006; Gullberg et al. 2016; Swinbank et al. 2015), detections of extended C IV and He II are elusive around QSOs and at LABs (e.g. Arrigoni Battaia et al. 2015a,b), and only compact detections of these lines have been found (e.g. Dey et al. 2005; Christensen et al. 2006; Prescott et al. 2009, 2013; Scarlata et al. 2009; Yang et al. 2010). The emission in C IV and He II is expected to be fainter than the Lyα emission on large scales in all the aforementioned scenarios (Yang et al. 2006; Arrigoni Battaia et al. 2015a,b; Cabot et al. 2016), and consequently only the brightest compact emission can currently be detected given the surface brightness limits achieved so far. We note that Prescott et al. (2012) argue that their non-detection of He II in narrowband imaging suggests extended emission of He II around a LAB.

In this work, we report the discovery of one of the first multiply lensed LABs. Located behind the *Hubble* Frontier Fields (HFF; P.I.: J. Lotz, see Lotz et al. 2016) cluster Abell S1063 (AS1063), it is one of the intrinsically-lowest luminosity LABs found to date, and the faintest to also show C IV and He II emission. We will demonstrate that the properties of this LAB are consistent with resonant scattering of an embedded star-forming source, shedding light on the origin of faint LABs. The layout of this paper is as follows. We present the data and method in Sect. 2, our results in Sect. 3, and our conclusions in Sect. 4. Throughout this work we use the standard flat ΛCDM cosmology, with $H_0 = 70$ km s^{-1} Mpc^{-1} and $\Omega_M = 0.3$, we use a Chabrier initial mass function (IMF), and all magnitudes refer to the AB system.

2. Methodology

2.1. Data

We observed AS1063 with the Multi Unit Spectroscopic Explorer (MUSE, Bacon et al. 2010) mounted on the Very Large Telescope (VLT) at Paranal for a total of three hours of exposure time. The observations were collected as part of the Science Verification, and the data are presented in Karman et al. (2015). We refer the reader to that work for a description of the data reduction, of which provide a quick overview here. The data was reduced with the standard pipeline version 0.18.2 and we verified that using a later version does not make a significant difference. The final datacube covers a field of 1 arcmin^2 in the south-west half of AS1063, and spans a spectral range of 4750 through 9350 Å. The spectral resolution of the MUSE instrument increases from $R \approx 1700$ at the blue to $R \approx 3500$ at ~9000 Å, which is enough to spectrally resolve the shape of Lyα emission. The seeing during the observations varied between 1.0″ and 1.1″ measured in white light, which corresponds to a FHWM of five to six pixels.

We re-examined the datacube after the first publication, inspecting specifically those positions with photometrically determined multiple images. We reported in Caminha et al. (2016) the redshifts of two new multiply lensed sources, of which one is an extended Lyα source, i.e. the LAB studied in this work, see Fig. 1. We extracted spectra at the positions of the multiple images within our field of view, α = 22:48:44.98; δ = −44:32:19.1

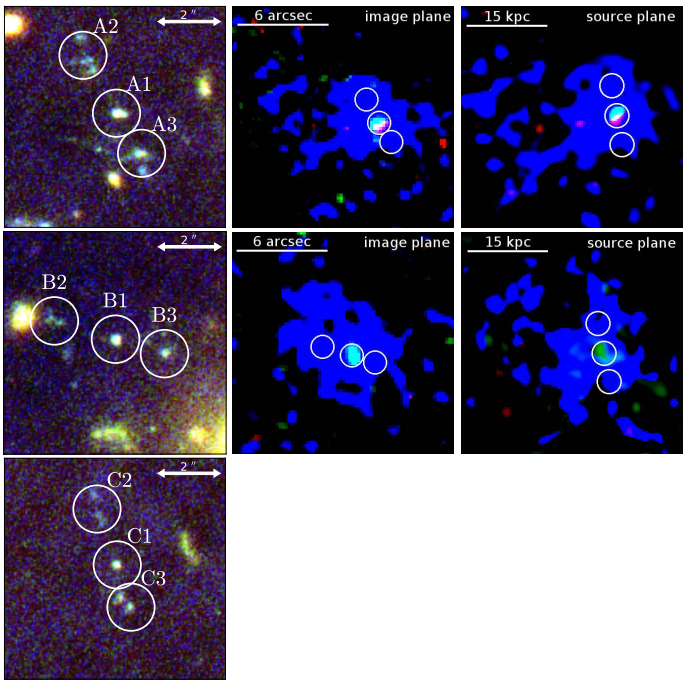

Fig. 2. *Left panels*: details of the LAB multiple images in the HFF colour composite image using the HST/ACS *F435W*, *F606W* and *F814W* filters. The circles have 0.″75 radius showing the compact source in the centre (ID 1) and the filamentary substructure (IDs 2 and 3). *Central panels*: colour composite images using the Lyα, C IV and He II emissions (blue, green and red channels, respectively) of the two LAB in the MUSE footprint, with a smooth kernel of 1″. *Right panels*: projected emissions onto the source plane. Note that the multiple images C are outside of our MUSE observations, and therefore we cannot show the corresponding Lya image reconstruction.

and α = 22:48:42.91; δ = −44:32:09.0, with differently sized apertures, to constrain the size and extent of this emission.

2.2. Strong lens model

This LAB is multiply lensed into three multiple images (A, B and C, see Fig. 2) and highly distorted and magnified by the gravitational potential of the foreground galaxy cluster AS1063. To compute the intrinsic properties of the LAB we corrected the observations from the strong lensing effect. We used an updated model of our previous strong lensing model ID F1-5th, presented in Caminha et al. (2016) to map the quantities between the source and image (observed) planes. We improved this model by fixing the redshift of the Lyα blob and we included two extra multiple images (structures of the Lyα blob) identified in the HFF images. We show these new multiple images in Fig. 2, identified as A2, A3, B2, B3, C2 and C3, see Table 1 for their coordinates. The multiple images A1, B1 and C1 correspond to the first identified compact source in the centre of the LAB considered in Caminha et al. (2016), and have *Hubble* Space Telescope (HST) *F814W* magnitudes of 25.39, 25.81, and 26.38, respectively (see Karman et al. 2016). The morphology, parity and colours of these substructures in all the three multiple images (A, B and C) are in full agreement with basic gravitational lensing theory, which ensures these substructures are at the same redshift. In this model we used only spectroscopically confirmed families, totalling 30 multiple images belonging to ten multiple image families of which eight are at different redshifts. The mean offset between the observed and model predicted positions of the images (A1, B1, C1), (A2, B2, C2) and (A3, B3, C3), is ≈0.″1, ensuring that our model reproduces the intrinsic properties of these sources very well. The multiple images A and B are in the MUSE footprint and the mean magnification factors over the extended region of the Lyα emission are 6.1 ± 0.5 and 5.0 ± 0.4, respectively. This corresponds to a delensed *F814W* magnitude of 27.36 and 27.56 for Images A1 and B1, respectively.

We used our strong lensing model to map the emission in the image plane onto the source plane, central and right panels of Fig. 2, respectively. In the case of Image B, the presence of nearby bright cluster members affects the reconstruction on the source plane significantly, making it more noisy than the reconstruction of Image A. We note that the observational seeing, not taken into account in this projection, might affect the shape of small scale features on the source plane. In both reconstructions in the source plane the extended nature of the Lyα emission remains and extends up to ≈33 kpc.

Table 1. Positions of the multiple images associated to the LAB (IDs A, B and C) and the positions (IDs N) throughout the nebula for which we extracted the spectra.

ID	α	δ
A1	22:48:44.98	−44:32:19.1
A2	22:48:45.05	−44:32:17.9
A3	22:48:44.92	−44:32:20.5
B1	22:48:42.91	−44:32:09.0
B2	22:48:43.09	−44:32:08.6
B3	22:48:42.78	−44:32:09.6
C1	22:48:40.96	−44:31:19.5
C2	22:48:41.01	−44:31:18.0
C3	22:48:40.92	−44:31:21.0
N1	22:48:45.08	−44:32:19.8
N2	22:48:44.88	−44:32:18.8
N3	22:48:45.21	−44:32:18.9

3. The multiply lensed Lyman-α blob

We found several emission lines in the spectra of compact sources A1 and B1 at the centre of the LAB, which we identified as Lyα, C IV$\lambda\lambda$1548,1551 Å, He IIλ1640 Å, and O III]1666 Å, determining the redshift to be z = 3.117. We show the Lyα, C IV, He II, and O III] emission lines of spectra of Image A1 in Fig. 3.

We used the integral field capabilities of MUSE to study the spatial profile of Lyα , and found a significantly extended emission area, see Fig. 1 and the central and right panels of Fig. 2. In Fig. 2, the Lyα emission of each multiple image appears to be extended up to ≈10″ on the image plane and ≈33 kpc on the source plane. In Fig. 1, we show the contours of the broad spatial Lyα emission, overplotted on a colour composite image constructed from the HFF images. From this image, we identified three compact sources embedded within the Lyα emission, which are shown in detail in the left panels of Fig. 2. One of these compact sources is very bright and lies at the centre of the emission while the other two present a filamentary structure. These two other sources are seen around all three multiple images, meaning that they are at a similar redshift. They are close enough to the central galaxy that they fall within the projected area of the Lyα emission. We note that the contours corresponding to the highest flux levels are located around images A1 and B1, rather than on top of it.

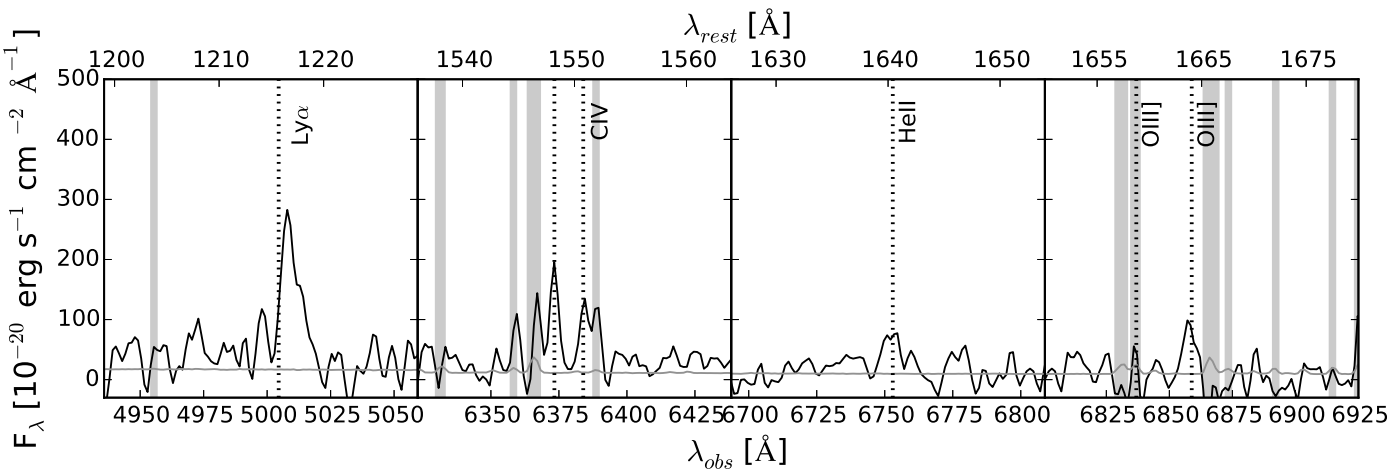

Fig. 3. Spectrum of the LAB Image A1 extracted with a circular aperture with 1″ radius, zoomed in on Lyα, C IV, and He II *from left to right*. The black line shows the spectrum, the grey line shows the typical error, the grey vertical bands are located at wavelengths with significant sky interference, and the dotted vertical lines show the location of the restframe emission lines.

The shape of the Lyα profile can give us insight into the properties of the gas surrounding this galaxy (e.g. Verhamme et al. 2008; Gronke et al. 2015). At the position of the brightest counterpart, the Lyα line has a typical asymmetric profile with a red tail and a small blue second peak separated by ~600 km s^{-1} from the red peak which is offset by ~200 km s^{-1} from the wavelength predicted from the ultraviolet (UV) emission lines. This line profile suggests a shell of gas flowing out of the galaxy at moderate velocity. We extracted spectra at the positions of these companions (IDs A2 and A3) and the central compact object (ID A1) finding no significant difference in the Lyα profile, see the top row of Fig. 4, or any emission line at other wavelengths. This means that these two sources are not bright enough in Lyα to be detected or distinguished from the Lyα nebula by our observations. Moreover, the Lyα profile at different positions of the nebula is very homogeneous, with no significant velocity offsets from the central position. This was also found by previous studies (Swinbank et al. 2007; Patrício et al. 2016), and indicates that the kinematic conditions of the nebula are similar in all directions. It is interesting to note that a deficit of the Lyα emission is seen close to the position of the bright central source, where the contours present a "valley". This is also illustrated in Fig. 4, where we compare the Lyα line at the bright central object A1 to other positions throughout the nebula. In addition to Image A1, we show the spectra at the other detected objects A2 and A3, and three positions without any optical counterpart. We chose N1 to be situated at the peak of Lyα flux, that is offset from A1, while positions N2 and N3 are chosen to sample the whole nebula. The peak of Lyα flux is less at A1 than at N1, and comparable to the other regions N2 and N3. The coordinates of these positions are shown in Table 1. We showed in the foregoing analysis that this is most probably due to gas Lyα transfer processes and not to the presence of dust.

The C IV doublet is clearly detected, and shows a narrow line profile, while the He II line is detected at ~4.8σ and is broader. The width of the C IV lines remains unresolved, meaning that the width is equal to the instrumental resolution, while the signal to noise of the He II lines is too low to reliably measure its width. Although broad emission lines would indicate AGN activity (but see Crowther et al. 2006, for broad emission lines in Wolf-Rayet stars), narrow emission lines can be produced by both AGN and SF.

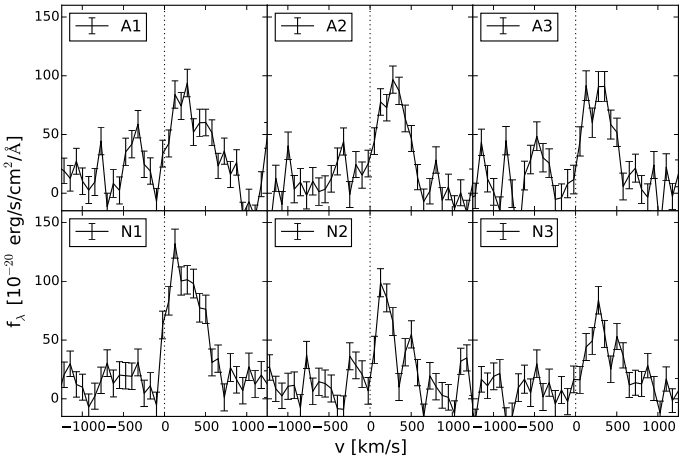

Fig. 4. Lyα profile at different positions of the nebula. The *top row* shows the Lyα line at the HST counterparts A1, A2, and A3, while three positions throughout the nebula are shown by N1, N2, and N3. The spectra have been summed within a four pixel apperture radius and the coordinates are shown in Table 1.

To investigate the powering source of the LAB, we studied the extent of the different emission lines. In the left panel of Fig. 5, we show the intrinsic cumulative flux profile as a function of the radius on the source plane for the two images integrating in the range of each emission and subtracting the continuum. The Lyα, C IV and He II emission fluxes are the circles, diamonds and stars, respectively. The flux centred on Image B1 is rescaled to account for the flux ratio anomalies that can be caused by small mass substructures not included in the lens model (Kochanek 1991; McKean et al. 2007). To highlight the extended nature of the emission, the grey lines show the shape of a Gaussian point source in similar seeing conditions.

It is clear from these figures that the Lyα emission is extended, while the C IV line is significantly more compact than the Lyα and cospatial with Source 1. This suggests that the nebula is not powered by photoionization or shocks. The extent of the He II line is more difficult to determine, as the flux density is low. Therefore, we cannot distinguish between gravitational

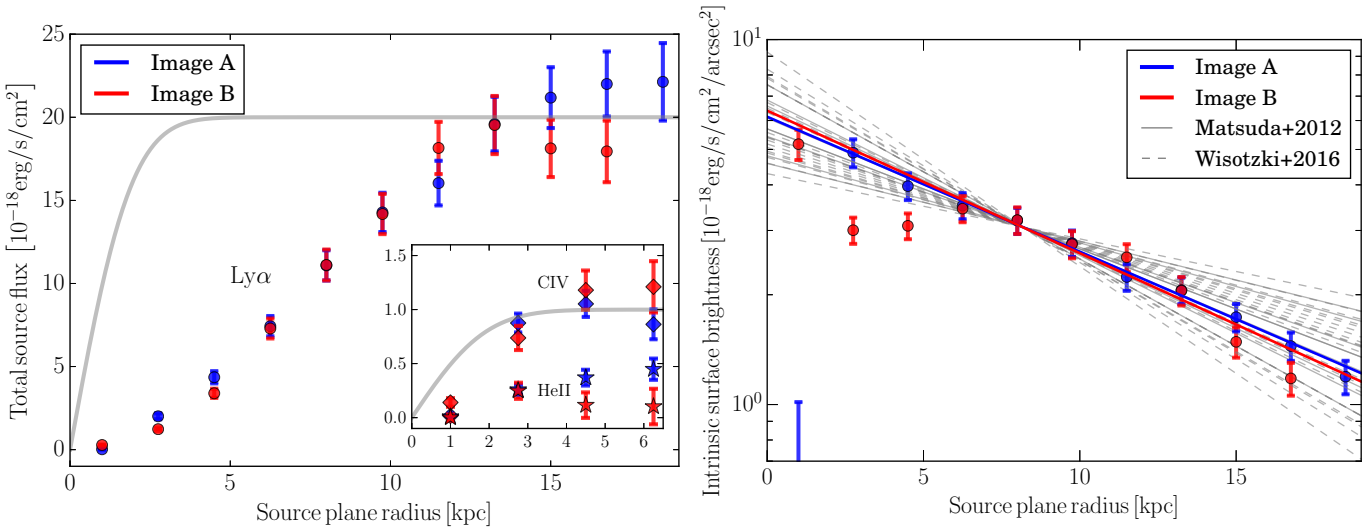

Fig. 5. *Left panel*: total flux on the source plane of the two multiple images of the LAB within the MUSE footprint, i.e. A1 and B1. The circles are the Lyα emission. In the *inset plot* we show the C IV and He II emissions, diamonds and stars respectively (the units are the same as in the main plot). The grey lines show the theoretical shape on the source plane of a Gaussian emission with observed scale of 1.″1 and arbitrary total flux. *Right panel*: intrinsic Lyα surface brightness. The red and blue lines indicate the best fit of an exponential function (considering the points $r > 5$ kpc, see text for details). The grey solid and dashed lines are the results from Matsuda et al. (2012) and Wisotzki et al. (2016), respectively, renormalized to $r = 8$ kpc.

cooling or resonant scattering, although the presence of a compact ionizing source suggests the latter.

In the right panel of Fig. 5, we show the Lyα surface brightness of sources A1 and B1 as a function of the radius on the source plane. The best fit, considering the scale of the surface brightness with the radius (r) given by $S(r) = C\exp(-r/r_n)$, where C is a normalization and r_n gives the slope of the curve, is shown in the figure. To avoid systematics in the fitting we excluded the points with $r < 5$ kpc for which the area is small and the measured flux more noisier and the observational seeing might contribute significantly in the overall slope. The best fitting values of r_n for the Images A1 and B1 are (11.8 ± 0.4) kpc and (11.1 ± 1.3) kpc, respectively. These values show good agreement with the measured slopes in Matsuda et al. (2012) and Wisotzki et al. (2016), also shown in the figure, although our Lyα surface brightness profile falls in the fainter range of these two samples and we cannot extend our fit to large radii due to the low surface brightness.

The ratio of Lyα to C IV or He II is often used to determine the ionizing source of LABs, even though effects on the Lyα emission like dust absorption could bias these ratios. In Fig. 6 we show our data together with the detections reported in the literature for Lyα nebulae at comparable redshift (Heckman et al. 1991; Villar-Martín et al. 2007; Prescott et al. 2009, 2013). In particular, we measured C IV/Lyα $= 0.44 \pm 0.12$ and He II/Lyα $= 0.12 \pm 0.05$ from a central region of 0.″5, and C IV/Lyα $= 0.16 \pm 0.03$ and He II/Lyα $= 0.03 \pm 0.01$ over the complete nebula, see Fig. 6. We see that the ratio of C IV/Lyα is high for its given He II/Lyα, and that the other LABs have a much lower C IV/Lyα ratio, while He II/Lyα is similar. This specific line ratio in the inner parts is in agreement with an AGN, while the ratio of the total nebula indicates SF as the main source of the Lyα emission (Binette et al. 2006; Villar-Martín et al. 2007; Swinbank et al. 2007), making it necessary the use of the O III emission to discriminate between these two scenarios. This shows the importance of integral field spectroscopy when studying ionization sources.

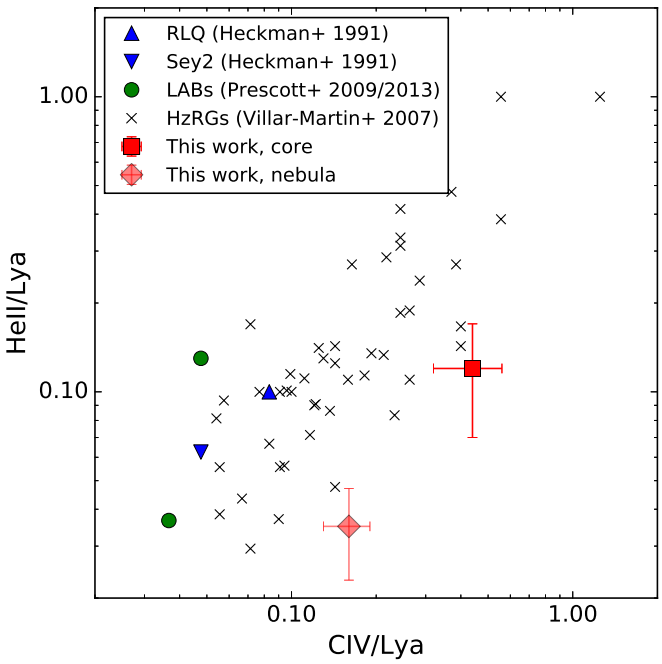

Fig. 6. Flux ratio of He II/Lyα versus C IV/Lyα. The red square corresponds to the central region of the Lyα emission, while the red semi-transparent diamond corresponds to the full nebula. We compare our results to the values found in other LABs (green circles, Prescott et al. 2009, 2013), HzRGs (black crosses, Villar-Martín et al. 2007), and radio loud quasars and Seyfert 2 hosts (blue triangles, Heckman et al. 1991).

Recently, Feltre et al. (2016) published predictions of UV line ratios for AGNe and SF galaxies. Unfortunately, one of the main lines that they discuss to separate dominant AGN from SF galaxies and determine ionization properties is C III], which we did not detect due to skylines. Alternatively, they show that the ratio of O III]/He II is able to separate AGNe and SF galaxies for most values. We measured Log(O III]/He II) $= 0.35 \pm 0.23$ in

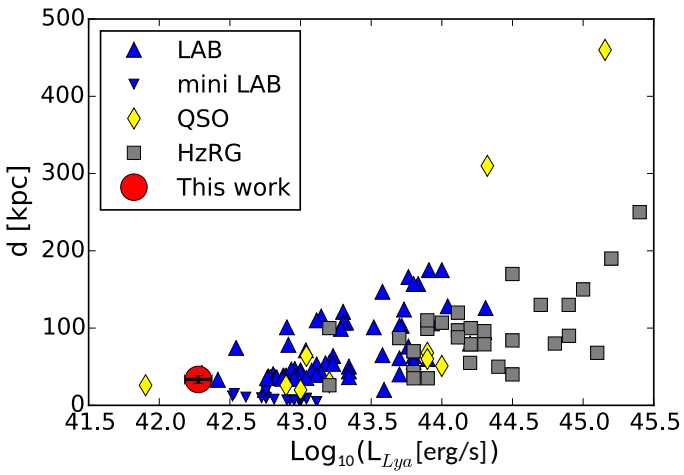

Fig. 7. Luminosity and diameter of our target compared to literature values. The LAB sample is taken from Matsuda et al. (2004, 2011), Ouchi et al. (2009), Prescott et al. (2013), and Patrício et al. (2016), the mini-LABs (d < 30 kpc) are from Saito et al. (2006, 2008), the HzRGs are from Heckman et al. (1991) and Swinbank et al. (2015), and the QSOs are taken from Christensen et al. (2006), North et al. (2012), Cantalupo et al. (2014), and Hennawi et al. (2015).

the central source, which indicates that SF is the dominant ionizing source in the core of the LAB. All other possible line ratios we were able to measure are consistent with SF being the dominant factor. To exclude possible AGN dominance, we ran a set of CLOUDY (last described by Ferland et al. 2013) models following Arrigoni Battaia et al. (2015a). We found that AGN-powered nebula have $-5.34 < \mathrm{Log(O\,III]/He\,II)} < -1.43$, which is incompatible with the ratio measured for the central region discussed here.

We compare the intrinsic luminosity of this source to other LABs and nebulas reported in the literature in Fig. 7. Clearly, the LAB studied here is one of the faintest nebula observed to date, and the faintest for which other emission lines are detected. We used $L_{\mathrm{Ly}\alpha}$ of the complete nebula to estimate the SF rate (SFR), assuming case B recombination and the conversion of Hα to SFR from Kennicutt (1998), and found $SFR_{\mathrm{Ly}\alpha} \approx 1.7\ M_{\odot}\ \mathrm{yr}^{-1}$. We note that case B recombination is not occuring in the nebula, but only in the central star forming region. We assume that the escaping Lyα photons are then scattered without significant absorption through the nebula to cause the extended emission.

We performed spectral energy distribution (SED) fitting on the broadband photometry from 0.4 through 2.4 μm to determine the stellar mass, stellar age, and SFR (see Karman et al. 2016). We only considered images A1 and C1, as the photometry of Image B is contaminated by nearby galaxies in several bands. We find a stellar mass of $\mathrm{Log}(M_{\star}) = 7.94^{+0.20}_{-0.16}$ ($7.85^{+0.20}_{-0.12}$) for images A (C). The SFR and stellar age are less constrained, with best fit values of $SFR = 2^{+18}_{-0.4}$ ($2.5^{+250}_{-1.5}$) $M_{\odot}\ \mathrm{yr}^{-1}$ and Log(age/yr) = $6.6\ ^{+1.4}_{-0.1}$ ($5.8^{+2.2}_{-0.4}$), finding good agreement between $\mathrm{SFR}_{\mathrm{Ly}\alpha}$ and $\mathrm{SFR}_{\mathrm{SED}}$. The galaxy is best fit by dust-poor templates, with $E(B-V) \leq 0.2$, showing that the central Lyα extinction is more likely due to transfer processes than dust absorption. We used the best-fitting SED to estimate the continuum flux, and derived an equivalent width of 110 Å for Lyα , which can be produced by SF (e.g. Charlot & Fall 1993). From the best-fitting SED, we measure a UV continuum slope $\beta = -2.09^{+0.06}_{-0.10}$ ($-2.18^{+0.08}_{-0.22}$). A young star-forming galaxy is in agreement with the UV line ratios, and we showed that it could be the source producing the scattered Lyα photons. Although the SED fitting (UV slope) does not suggest large amounts of dust, we cannot exclude some dust attenuation of the Lyα emission and hence an underestimate of the SFR. We note however that the inclusion of little dust would not affect our conclusions about the nature of the luminosity of the nebula.

From the left panels of Fig. 2 we see that the continuum light of sources A1, B1, and C1 is spatially resolved. We measured an effective radius of 0.″11, corresponding to a physical scale of ~360 pc. Because most of the light is emitted in this resolved region, most of the light cannot be due to an unresolved point source, for example an AGN. This further strengthens our conclusion that SF is producing the scattered Lyα photons, rather than an AGN.

In the MUSE footprint we found two other compact Lyα emitters at the same redshift ($z = 3.117$), one is also a multiply lensed galaxy and optically-thin (red circles in Fig. 1, and a possible Lyman continuum emitter, see Vanzella et al. 2016), and the other is reported in Table 2 of Karman et al. (2015). Vanzella et al. (2016) showed also that the optically-thin source is very young, dust-free and low mass object, belonging to a low-luminosity domain, $L_{1500} \approx 0.02L^{*}_{z=3}$, possibly analogue to the sources responsible for reionization. The distance between these three objects on the source plane is $\lesssim$103 kpc, indicating that the LAB is located in a group of galaxies, and possibly a protocluster.

It is noteworthy that besides the LAB presented here, the only other multiply lensed LAB (Patrício et al. 2016) also shows a relatively small and faint Lyα nebula powered by SF, although it is significantly more massive than the LAB discussed here. These faint LABs powered by SF are very similar to those obtained in the local Universe, as found by the Lyman Alpha Reference Sample (Hayes et al. 2013), and indicate that with the new generation of IFUs in combination with gravitational lensing we are now probing the CGM of sub-L_{*} galaxies at $z \sim 3$.

4. Conclusions

In this work, we presented the discovery of a faint multiply lensed LAB. Using MUSE, we obtained spectral and spatial information on the Lyα, C IV, He II, and O III] lines, which we used to determine the powering source of this LAB. We used our gravitational lensing model to correct for magnification and to reconstruct intrinsic source properties.

We found an extended Lyα emission region, with a total luminosity of 1.9×10^{42} erg s^{-1} distributed over a circular area with a radius of 16.5 kpc on the source plane. The low luminosity makes this Lyα nebula the second faintest observed to date, and the faintest LAB with detected UV emission lines.

Besides Lyα, we found no other lines with extended emission, although the He II flux density is too low to exclude extended emission. Unlike He II, the flux density of the C IV emission is high enough to rule out extended emission, which indicates that photoionization or shocks cannot be the powering mechanism of this LAB. In addition, the deficit of Lyα at the centre of the LAB hints at resonant scattering rather than gravitational cooling. The UV-line ratios indicate that the embedded source in the LAB is SF rather than an AGN.

Interestingly, we confirmed spectroscopically two other galaxies at very close distance from the LAB. This is in agreement with previous results in the literature that show that LABs reside in overdensities (Yang et al. 2009). With dedicated observations in the future, one could quantify the galaxy overdensity and establish the presence of a protocluster behind AS1063.

Acknowledgements. G.B.C. is supported by the CAPES-ICRANet program grant BEX 13946/13-7. C.G. acknowledges support by VILLUM FONDEN Young Investigator Programme grant 10123. We acknowledge financial support from PRIN-INAF 2014 1.05.01.94.02. This work made use of the CHE cluster, managed and funded by ICRA/CBPF/MCTI, with financial support from FINEP (grant 01.07.0515.00 from CT-INFRA−01/2006) and FAPERJ (grants E-26/171.206/2006 and E-26/110.516/2012). This work also made use of data gathered under the ESO programmes 186.A-0798 and 60.A-9345(A).

References

Ao, Y., Matsuda, Y., Beelen, A., et al. 2015, A&A, 581, A132
Arrigoni Battaia, F., Hennawi, J. F., Prochaska, J. X., & Cantalupo, S. 2015a, ApJ, 809, 163
Arrigoni Battaia, F., Yang, Y., Hennawi, J. F., et al. 2015b, ApJ, 804, 26
Bacon, R., Accardo, M., Adjali, L., et al. 2010, in Ground-based and Airborne Instrumentation for Astronomy III, Proc. SPIE, 7735, 773508
Binette, L., Wilman, R. J., Villar-Martín, M., et al. 2006, A&A, 459, 31
Bridge, C. R., Blain, A., Borys, C. J. K., et al. 2013, ApJ, 769, 91
Cabot, S. H. C., Cen, R., & Zheng, Z. 2016, MNRAS, 462, 1076
Caminha, G. B., Grillo, C., Rosati, P., et al. 2016, A&A, 587, A80
Cantalupo, S., Arrigoni-Battaia, F., Prochaska, J. X., Hennawi, J. F., & Madau, P. 2014, Nature, 506, 63
Charlot, S., & Fall, S. M. 1993, ApJ, 415, 580
Christensen, L., Jahnke, K., Wisotzki, L., & Sánchez, S. F. 2006, A&A, 459, 717
Crowther, P. A., Hadfield, L. J., Clark, J. S., Negueruela, I., & Vacca, W. D. 2006, MNRAS, 372, 1407
Dey, A., Bian, C., Soifer, B. T., et al. 2005, ApJ, 629, 654
Dijkstra, M., & Loeb, A. 2008, MNRAS, 386, 492
Dijkstra, M., & Loeb, A. 2009, MNRAS, 400, 1109
Faucher-Giguère, C.-A., Kereš, D., Dijkstra, M., Hernquist, L., & Zaldarriaga, M. 2010, ApJ, 725, 633
Feltre, A., Charlot, S., & Gutkin, J. 2016, MNRAS, 456, 3354
Ferland, G. J., Porter, R. L., van Hoof, P. A. M., et al. 2013, Rev. Mex. Astron. Astrofis., 49, 137
Geach, J. E., Alexander, D. M., Lehmer, B. D., et al. 2009, ApJ, 700, 1
Gronke, M., Bull, P., & Dijkstra, M. 2015, ApJ, 812, 123
Gullberg, B., De Breuck, C., Lehnert, M. D., et al. 2016, A&A, 586, A124
Hayes, M., Scarlata, C., & Siana, B. 2011, Nature, 476, 304
Hayes, M., Östlin, G., Schaerer, D., et al. 2013, ApJ, 765, L27
Heckman, T. M., Miley, G. K., Lehnert, M. D., & van Breugel, W. 1991, ApJ, 370, 78
Hennawi, J. F., Prochaska, J. X., Cantalupo, S., & Arrigoni-Battaia, F. 2015, Science, 348, 779
Humphrey, A., Villar-Martín, M., Fosbury, R., Vernet, J., & di Serego Alighieri, S. 2006, MNRAS, 369, 1103
Karman, W., Caputi, K. I., Grillo, C., et al. 2015, A&A, 574, A11
Karman, W., Caputi, K. I., Caminha, G. B., et al. 2016, A&A, in press, DOI: 10.1051/0004-6361/201629055
Kennicutt, Jr., R. C. 1998, ARA&A, 36, 189
Kochanek, C. S. 1991, ApJ, 373, 354
Lotz, J. M., Koekemoer, A., Coe, D., et al. 2016, ApJ, submitted [arXiv:1605.06567]
Matsuda, Y., Yamada, T., Hayashino, T., et al. 2004, AJ, 128, 569
Matsuda, Y., Yamada, T., Hayashino, T., et al. 2011, MNRAS, 410, L13
Matsuda, Y., Yamada, T., Hayashino, T., et al. 2012, MNRAS, 425, 878
McKean, J. P., Koopmans, L. V. E., Flack, C. E., et al. 2007, MNRAS, 378, 109
Mori, M., & Umemura, M. 2006, New A Rev., 50, 199
Nilsson, K. K., Fynbo, J. P. U., Møller, P., Sommer-Larsen, J., & Ledoux, C. 2006, A&A, 452, L23
North, P. L., Courbin, F., Eigenbrod, A., & Chelouche, D. 2012, A&A, 542, A91
Ouchi, M., Ono, Y., Egami, E., et al. 2009, ApJ, 696, 1164
Overzier, R. A., Nesvadba, N. P. H., Dijkstra, M., et al. 2013, ApJ, 771, 89
Patrício, V., Richard, J., Verhamme, A., et al. 2016, MNRAS, 456, 4191
Prescott, M. K. M., Dey, A., & Jannuzi, B. T. 2009, ApJ, 702, 554
Prescott, M. K. M., Dey, A., Brodwin, M., et al. 2012, ApJ, 752, 86
Prescott, M. K. M., Dey, A., & Jannuzi, B. T. 2013, ApJ, 762, 38
Prescott, M. K. M., Momcheva, I., Brammer, G. B., Fynbo, J. P. U., & Møller, P. 2015, ApJ, 802, 32
Prochaska, J. X., Lau, M. W., & Hennawi, J. F. 2014, ApJ, 796, 140
Saito, T., Shimasaku, K., Okamura, S., et al. 2006, ApJ, 648, 54
Saito, T., Shimasaku, K., Okamura, S., et al. 2008, ApJ, 675, 1076
Scarlata, C., Colbert, J., Teplitz, H. I., et al. 2009, ApJ, 706, 1241
Steidel, C. C., Adelberger, K. L., Shapley, A. E., et al. 2000, ApJ, 532, 170
Steidel, C. C., Bogosavljević, M., Shapley, A. E., et al. 2011, ApJ, 736, 160
Swinbank, A. M., Bower, R. G., Smith, G. P., et al. 2007, MNRAS, 376, 479
Swinbank, A. M., Vernet, J. D. R., Smail, I., et al. 2015, MNRAS, 449, 1298
Vanzella, E., De Barros, S., Cupani, G., et al. 2016, ApJ, 821, L27
Verhamme, A., Schaerer, D., Atek, H., & Tapken, C. 2008, A&A, 491, 89
Villar-Martín, M., Vernet, J., di Serego Alighieri, S., et al. 2003, MNRAS, 346, 273
Villar-Martín, M., Humphrey, A., De Breuck, C., et al. 2007, MNRAS, 375, 1299
Wisotzki, L., Bacon, R., Blaizot, J., et al. 2016, A&A, 587, A98
Yamada, T., Nakamura, Y., Matsuda, Y., et al. 2012, AJ, 143, 79
Yang, Y., Zabludoff, A. I., Davé, R., et al. 2006, ApJ, 640, 539
Yang, Y., Zabludoff, A., Tremonti, C., Eisenstein, D., & Davé, R. 2009, ApJ, 693, 1579
Yang, Y., Zabludoff, A., Eisenstein, D., & Davé, R. 2010, ApJ, 719, 1654